Available online at www.sciencedirect.com
ScienceDirect
Journal of Molecular Graphics and Modelling 26 (2007) 117–123
Journal of Molecular Graphics and Modelling
www.elsevier.com/locate/JMGM

CoMFA based *de novo* design of pyridazine analogs as PTP1B inhibitors

Pramod C. Nair, M. Elizabeth Sobhia *

Centre for Pharmacoinformatics, National Institute of Pharmaceutical Education and Research (NIPER), Sector 67, S.A.S. Nagar, Punjab 160062, India

Received 6 July 2006; received in revised form 5 October 2006; accepted 18 October 2006
Available online 24 October 2006

Abstract

PTP1B plays an important role as a negative regulator in insulin and leptin signaling pathways. Potent and orally active PTP1B inhibitors can act as potential agents for the treatment of Type 2 diabetes and obesity. CoMFA (Comparative Molecular Field Analysis) and *de novo* ligand design using LeapFrog (LF) studies were performed on pyridazine analogs, reported to be selective and non-competitive inhibitors of PTP1B. A robust model was developed which produced statistically significant results with cross-validated and conventional correlation coefficients of 0.619 and 0.990, respectively. Further, the robustness of the model was verified by bootstrapping analysis. LeapFrog (LF) program is a *de novo* drug discovery tool, which uses CoMFA maps to generate hypothetical cavity and ligands. As the crystal structure of PTP1B–pyridazine complex is not yet known, the contours of CoMFA model was used to serve as a pharmacophoric model to generate hypothetical cavity for LeapFrog calculations. Ligands were optimized using this concept.

Keywords: Insulin and leptin signaling; Type 2 diabetes; Obesity; PTP1B; CoMFA; LeapFrog

1. Introduction

Type 2 Diabetes Mellitus (T2DM), the most common form of diabetes represents 90% of the diabetic population. It is caused by the resistances to the action of insulin combined with a deficiency in insulin secretion. In the current scenario of diabetic research, metformin and thiazolidinediones class of compounds are the only agents that address the aspects of insulin resistance [1,2]. Hence increasing awareness of the clinical implications of insulin resistance and increasing knowledge of the cellular basis of insulin resistance [2] provides the rationale and a means for developing an anti-insulin resistance approach to the treatment of T2DM. Inhibition of protein tyrosine phosphatase 1B (PTP1B) has emerged as an attractive approach in this direction for addressing the issue of insulin resistance [2]. PTP1B plays an important role as a negative regulator in the insulin and leptin signaling pathways [3,4]. Two laboratories have independently proved that PTP1B knockout mice showed increased sensitivity to insulin in skeletal muscle and liver, increased insulin receptor auto phosphorylation and resistance to weight gain [3,5,6]. These studies suggest that inhibition of PTP1B may be effective for the treatment of type 2 diabetes and obesity.

There are many challenges in developing inhibitors for PTP1B, which include selectivity, permeability, design of low molecular weight ligands and design of non-peptidic inhibitors [7]. Among these concerns, selectivity has been the major focus of researchers in the recent years and a few novel selective PTP1B derivatives have come out of these efforts. However, their clinical efficacy for therapeutic usage in reference to the above-mentioned challenges is questionable [8–15]. Here, we present the results of CoMFA (Comparative Molecular Field Analysis) and LeapFrog (LF) calculations carried out on pyridazine analogs, reported to be selective inhibitors of PTP1B. Pyridazine analogs belong to the class of non-competitive inhibitors, which may bind to a site other than the active site of a protein molecule. Recent studies carried out

* Corresponding author. Tel.: +91 172 2214 682x2025; fax: +19 172 2214 692.
E-mail addresses: mesophia@niper.ac.in, e_sophia1@yahoo.co.in (M.E. Sobhia).

1093-3263/$ – see front matter © 2006 Elsevier Inc. All rights reserved.
doi:10.1016/j.jmgm.2006.10.002

using Computer Aided Drug Design (CADD) methods on PTP1B inhibitors comprise: CoMFA based docking studies on diverse human PTP1B inhibitors by Taha and AlDamen [16], 3D-QSAR studies on 2-(oxalylamino) benzoic acid analogs by Zhou and Ji [17], CoMFA and CoMSIA studies on protein tyrosine phosphatase 1B inhibitors by Murthi and Kulkarni [18] and CoMSIA study on 1,2-naphthoquinone derivatives by Sobhia and Bharatam [19]. As far as the non-competitive inhibitors are concerned, only very few QSAR studies have been carried out including the one being recently reported by Martinez et al. on 2,4-disubstituted thiadiazolidinones (TDZD), described as the ATP-non competitive GSK-3 inhibitors [20]. We report here the results of our preliminary investigations carried out on pyridazine analogs using CoMFA and LeapFrog. LeapFrog [21] is a *de novo* tool, which makes use of the CoMFA contours for the generation of hypothetical cavity and optimization of ligands. Studies based on LeapFrog calculations have been reported in the literature [22,23].

2. Computational details

2.1. Dataset for analysis

In vitro inhibitory activity data (IC_{50} μM) of the pyridazine analogs on PTP1B, reported by Liljebris et al. [24] was taken for the study. Inhibitory activity was determined using pNPP as the substrate [24]. Out of 41 PTP1B inhibitors which were reported, 37 molecules were selected for developing the model and four molecules whose IC_{50} values reported as >100 were not considered for the study. The dataset was randomly segregated into training and test set comprising 28 and 9, respectively. The IC_{50} (μM) values were taken in molar (M) range and converted to pIC_{50} according to the formula.

$$pIC_{50} = -\log IC_{50}$$

2.2. Molecular modeling

All molecular modeling studies were performed using the molecular modeling package SYBYL7.1 [25] installed on a Silicon Graphics Fuel Work station. Since the crystal structure of PTP1B–pyridazine complex is not yet reported the most active molecule in the training set was chosen as the template and the rest of the molecules were derived from it. Tripos force field and Gasteiger–Huckel partial atomic charges were used for minimizing the molecules [26]. Powell's conjugate gradient method was used for minimization [27]. The minimum energy difference of 0.001 kcal/mol was set as a convergence criterion.

2.3. Alignment rule

Alignment being the sensitive part of the CoMFA analysis, alignment using a common template was carried out to overlay the molecule appropriately in one possible orientation. The pyridazine molecules are reported to be non-competitive inhibitors, hence not expected to bind at the catalytic binding site [4]. Also the crystal structure of PTP1B with such analogs are not available, an assumption was made from the SAR studies that the phenyl substituted pyridazine based bicyclic nucleus plays a key role in binding at a non-catalytic site and it was taken for alignment. Molecule 36 was taken as the template and rest of the molecules were aligned to it using FIT atom method in SYBYL. Eight atoms were selected for superimposition and the common sub structure is shown in Fig. 1a. The aligned molecules are shown in Fig. 1b.

2.4. CoMFA interaction energies

CoMFA samples the steric and electrostatic fields surrounding a set of ligands and constructs a 3D-QSAR model by correlating these 3D fields with the corresponding biological/experimental activities [28].

The steric and electrostatic CoMFA potential fields were calculated at each lattice intersection of a regularly spaced grid of 2.0 Å. The grid box dimensions were determined automatically in such a way that the region boundaries were extended beyond 4 Å in each direction from the co-ordinate of each molecule. The van der Waals potential and Coulombic terms, which represent steric and electrostatic fields, respectively, were calculated using the standard Tripos force fields. A distance dependent dielectric constant of 1.00 was used. An sp^3 hybridized carbon atom with +1 charge served as probe atom to calculate steric and electrostatic fields. The steric and electrostatic contributions were truncated to +30.0 kcal/mol and electrostatic contributions were ignored at the lattice intersections with maximal steric interactions.

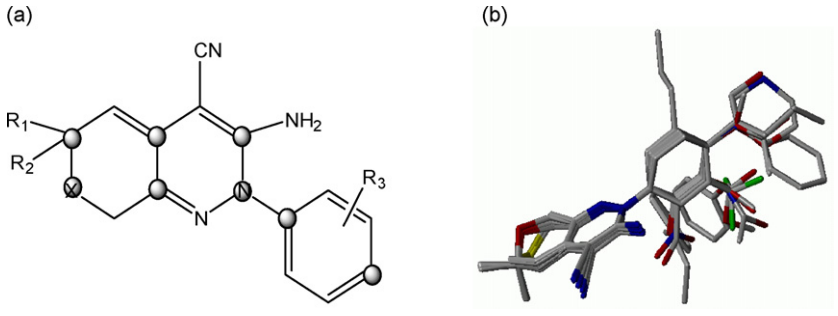

Fig. 1. (a) Schematic diagram showing the atoms used for fit atom alignment and (b) alignment of the training set molecules.

2.5. Partial least square (PLS) analysis

PLS method [29] was used to linearly correlate the CoMFA fields to biological activity values. The cross-validation was performed using leave-one-out (LOO) method in which one compound is removed from the dataset and its activity is predicted using the model derived from the rest of the molecules in the dataset. Equal weights for CoMFA were assigned to steric and electrostatic fields using CoMFA STD scaling option. To speed up the analysis and reduce noise, a minimum column filter value (r) of 2.00 kcal/mol was used for the cross-validation. Non-cross-validation was performed to calculate conventional r^2 (r^2_{ncv}) using the same number of components. To further assess the robustness and statistical confidence of the derived models, bootstrapping analysis for 100 runs was performed [29,30]. Bootstrapping involves the generation of many new data sets from original data set and is obtained by randomly choosing samples from the original data set. The statistical calculation is performed on each of these bootstrapping samplings. The difference between the parameters calculated from the original data set and the average of the parameters calculated from the many bootstrapping samplings is a measure of the bias of the original calculations. The entire cross-validated results were analyzed considering the fact that a value of r^2_{cv} above 0.3 indicates that probability of chance correlation is less than 5% [29].

2.6. Hypothetical cavity generation using LeapFrog

LeapFrog is a *de novo* tool to design a series of potential active ligand molecules even when the receptor structure is unknown [21]. As the crystal structure complex of PTP1B with pyridazine analogs is not determined; we have used this *de novo* tool for proposing new molecules as potential inhibitors of PTP1B. Binding energy calculations in LeapFrog are performed by three major components viz., direct steric, electrostatic, and implicit hydrogen bonding enthalpies of ligand–cavity binding using the Tripos force field. The method of calculating binding energies in LeapFrog is similar to that of Goodford's GRID program [31]. However, in LeapFrog, ligand atom coordinates are binned to increase speed and the binding energy of each ligand atom is calculated as though the atom were actually located in the center of a cube containing that atom. A simple linear expression then yields the energy of interaction between the site and that particular ligand atom. Summing over all ligand atoms yields the overall site–ligand interaction energy. The program also allows use of optional cavity desolvation energy, an optional incremental hydrogen bonding energy, and optional ligand desolvation energy, estimated from a very simple model.

LeapFrog makes use of the CoMFA contours for the generation of its cavity. There are two distinct ways to perform this process. One is by direct point-by-point mapping of the properties of a CoMFA grid to an intermediate cavity grid of the same coarse resolution, and the other is by interpolation of the intermediate cavity grid values to the closely spaced grid values actually used by LF. The cavity thus obtained was used to generate the site points. The charge of a site point atom is positive, negative, or lipophilic. Its value is compared with 1.0. If the atom charge is smaller in magnitude than 1.0 the site point is lipophilic; if greater than +1.0, the site point seeks a negative atom; and if less than 1.0, the site point seeks a positive atom in the approaching fragment.

The results of PLS analysis described above and the region file of the contour was used to for cavity generation calculations for our study. The OPTIMIZE mode of the LeapFrog was used for optimization of the ligands. The molecules 10, 28, 38 were subjected to OPTIMIZE mode for their improvement in binding energy. Molecule 38 ($IC_{50} > 100$) was excluded from CoMFA analysis, as its activity was not given in exact numerals. However, this molecule was intentionally chosen for optimization studies using LeapFrog. WEED was performed immediately after the run of 100 moves which discards all ligands except the top n in binding score, where n was set to be 10 which is default number of ligands as per the SYBYL tailor set-up. CROSSOVER, a genetic move for generating the best hybridizations among these diverse structural changes was also performed. Within the top ligand having good binding energy, the most central of the interesting rotatable bonds is identified in the crossover. To identify the corresponding bond within the other ligands, a 2D search query is generated, based on the bound atoms plus all heavy atoms attached to this bond. Each ligand containing this 2D pattern is split into two half-fragments by breaking the identified bond. Half-fragments that are structurally identical to other half-fragments are discarded. All possible recombination of the remaining half ligands are then performed, using the SYBYL JOIN command while retaining the existing torsion setting followed by a FLY move without initial perturbations. Those which are successfully evaluated are kept, producing up to n $(n-1)/2$ ligands from the n ligands undergoing the CROSSOVER move [21].

3. Results and discussion

CoMFA model was obtained with 28 and 9 molecules in the training and test set respectively. Summary of the PLS analysis is shown in Table 1. The actual, predicted and residuals of the training set and test set molecules are shown in Tables 2 and 3, respectively. The plot of actual versus predicted pIC_{50} of training set molecules is shown in Fig. 2 and the histogram for the residuals of the test molecules is shown in Fig. 3. The molecules in the training and test set were examined for the outliers (Tables 2 and 3). The molecules having residual higher than 0.9 log unit were considered as outliers. Molecule 1 has residual value of 0.90; one of the possible reasons for it to be an outlier is that no molecule in the training set has C as atomic substituents at X of the bicyclic ring. The molecule 11 having residual value 0.93 was also not predicted well by the model. Different models were developed keeping this molecule in the training set and it was found that inclusion of this compound drastically disturbed the robustness of the model; no proper reasons could be attributed for the behavior of this molecule.

Table 1
Statistical parameters obtained from CoMFA study

Parameters	CoMFA
r^2_{cv} (LOO)	0.619
NOC	8
r^2_{ncv}	0.990
F	235.6
SEE	0.046
r^2_{cv}	0.630
$r^2_{boot\ strap}$	0.997
S.D.	0.003
Relative contributions	
Steric	0.68
Electrostatic	0.32

r^2_{cv} (LOO) = cross-validated correlation coefficient by Leave One Out; r^2_{cv} = cross validated correlation coefficient; r^2_{ncv} = non-cross validated correlation coefficient NOC = number of components; r^2 = conventional correlation coefficient; SEE = standard error of estimate; PRESS = predicted residual sum of squares of test set molecules, r^2_{pred} = predictive correlation coefficient, $r^2_{boot\ straps}$ = correlation coefficient after 100 runs of bootstrapping analysis, S.D. = standard deviation from 100 bootstrapping runs.

3.1. Contour interpretation

The contour maps obtained by CoMFA show how 3D-QSAR methods are useful to identify features important for recognizing protein–ligand interactions. The contour maps also give an indication of those portions of the molecule that require particular property to improve the binding affinity. The CoMFA steric interactions are represented by favoured green and disfavoured yellow contours while electrostatic interactions are represented by negative charge favoured red and positive charge favoured blue contours (Fig. 4). The most active molecule 36 (IC_{50} 0.35 μM) is displayed in the background of contours.

The contours of electrostatic fields reveal a quite a big red region near the phenyl ring of the template molecule and it is noted that many of the high active molecules like 15 (IC_{50} = 2.9 μM), 16 (IC_{50} = 2.2 μM), 32 (IC_{50} = 2.8 μM) and 37 (IC_{50} = 2.1 μM) have their electro negative groups encroached in this region. A small red polyhedron lies near the bicyclic nucleus of the template and three other small red contours are present surrounding the phenyl ring of the molecule where high electron density is expected to increase the activity. High active compounds direct their negative groups

Table 2
Actual, predicted inhibitory activities (pIC_{50}) and residuals of the training set molecules

S. no.	Molecule	Actual pIC_{50}	Predicted pIC_{50}	Residuals
1	3	5.70	5.70	0.00
2	4	5.70	5.80	−0.10
3	6	5.89	5.89	0.00
4	7	5.96	5.86	0.10
5	8	5.54	5.54	0.00
6	9	5.09	5.08	0.01
7	10	5.15	5.13	0.02
8	12	5.31	5.27	0.04
9	14	5.35	5.36	−0.01
10	15	5.54	5.53	0.01
11	16	5.66	5.60	0.06
12	17	5.21	5.22	−0.01
13	18	5.44	5.46	−0.02
14	19	4.64	4.65	−0.01
15	20	4.80	4.78	0.02
16	21	5.41	5.41	0.00
17	22	5.21	5.17	0.04
18	23	5.64	5.64	0.00
19	24	4.76	4.78	−0.02
20	25	5.55	5.62	−0.07
21	28	5.77	5.76	0.01
22	29	4.96	4.95	0.01
23	30	5.62	5.62	0.00
24	32	5.55	5.55	0.00
25	33	5.49	5.51	−0.02
26	35	5.24	5.32	−0.08
27	36	6.46	6.45	0.01
28	37	5.68	5.67	0.01

Table 3
Actual, predicted inhibitory activities (pIC_{50}) and residuals of the test set molecules

S. no.	Molecules	Actual pIC_{50}	Predicted pIC_{50}	Residuals
1	1	4.98	5.88	−0.90
2	2	5.25	6.08	−0.83
3	5	5.36	5.80	−0.44
4	11	5.82	4.89	0.93
5	13	5.62	5.20	0.42
6	26	5.80	4.97	0.83
7	27	5.09	5.68	−0.59
8	31	5.41	5.00	0.41
9	34	5.47	4.95	0.52

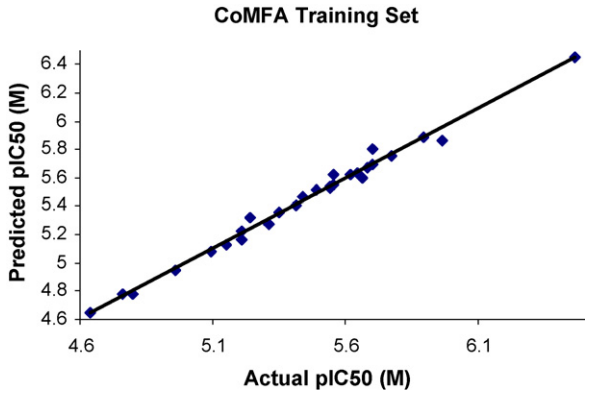

Fig. 2. Plot of actual vs. predicted pIC_{50} of the training set molecules.

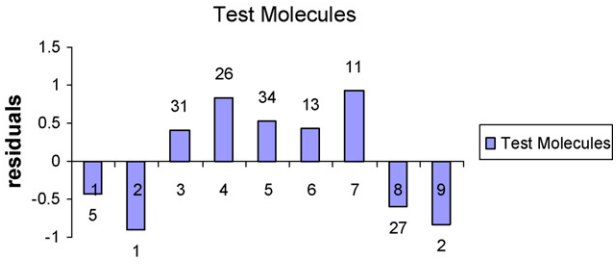

Fig. 3. Histogram of residuals of the test set molecules.

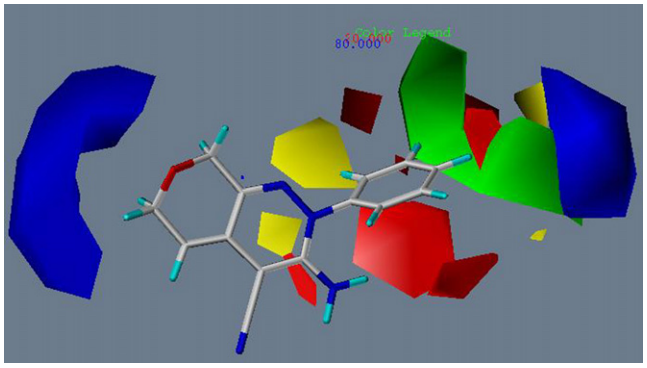

Fig. 4. CoMFA STDEVXCOEFF steric and electro static contour maps. The most active molecule 36 is displayed in the background.

and low active molecules point their positive groups in these regions. A prominent blue contour is present near the bicyclic ring of the template indicating that the electropositive groups at this position may increase the activity, as noted in many compounds having geminal dimethyl group (Table 4). Similarly, presence of green contour near the phenyl ring (Fig. 4) indicates that the substitution of a bulky moiety may increase activity as can be seen in the case of compound 28 (IC_{50} = 1.7 μM) having 4-CH_2OH substitution on the phenyl ring which is both electro negative as well as bulky. Compound 15 (IC_{50} = 2.9 μM) with 4-CH_2CH_2OH and Compound 16 (IC_{50} 2.2 μM) with a 4-methoxy substituents also follow the same trend. The bulky and electronegative group (3-$COOCH_3$) of compound 37 (IC_{50} = 2.1 μM) at the third position seems to be penetrating the junction of red and green contours indicating the presence of bulkiness as well as electro negativity for the enhancement of activity. Similar observation was found in case of compound 32 (IC_{50} = 2.8 μM) with group 3-CF_3. The contours for compound 33 (IC_{50} = 3.2 μM) showed that only the methyl tail of 4-OCH_2CH_3 was engulfed into the green contours indicating more bulkiness at that region would increase its activity. Comparatively less activity was seen in 20 (IC_{50} = 15.8 μM) as the bulky O–Ph at second position of phenyl ring was found to penetrate the yellow contours.

3.2. Analysis of LeapFrog calculations

The results of PLS analysis described above and the region file of the contour was used to for cavity generation calculations for our study. The OPTIMIZE mode of the LeapFrog was used for optimization of the ligands. The molecules 10, 28, 38 were subjected to OPTIMIZE mode for their improvement in binding energy. Molecule 38 (IC_{50} > 100) was excluded from CoMFA analysis, as its activity was not given in exact numerals. LeapFrog calculations were carried out for the optimization different ligands. The contours of CoMFA model were used to serve as a phramacophore model to generate hypothetical cavity for LeapFrog calculations. The results obtained for three reference molecules viz., 10, 28 and 38 are presented. Scheme 1 shows a set of optimized molecules along with reference molecules and LeapFrog binding energies. LeapFrog calculations were computationally validated by optimizing one of the poorly active molecule 38 (BE = −481.03 kcal/mol) to molecule 12(BE = −572.16 kcal/mol), which is reported in the dataset (Table 4). The site points generated by LeapFrog calculations are represented in different colors (Fig. 5), the blue spheres represent hydrogen bonding acceptor site points, the red spheres represent donor site points and the yellow spheres represent the lipophilic site points. Fig. 5 represents a view of the site points generated by LeapFrog and the most active molecule 36 is shown in the background. The optimized molecules have higher stable energy compared to the starting molecules. One of the optimized molecules O4, overlaid on CoMFA contours is shown in Fig. 6. The molecule O4 is shown in different colors; magenta shows the backbone of the reference molecule while Sybyl type atom colors show the

Table 4
Data set used in the study and their PTP1B activity (IC_{50})

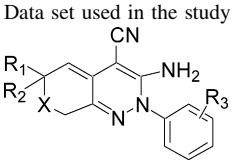

S. no.	Molecules	R_1	R_2	R_3	X	IC_{50} (μM)
1	1	H	H	H	C	10.4
2	2	H	H	4-iPropyl	S	5.6
3	3	H	H	2-iPropyl	S	2.0
4	4	H	H	4-F	S	2.0
5	5	H	H	2-F	S	4.4
6	6	H	H	4-OMe	S	1.3
7	7	H	H	H	S	1.1
8	8	CH_3	CH_3	2-Morpholinyl	O	2.9
9	9	CH_3	CH_3	3-iPropyl	O	8.2
10	10	CH_3	CH_3	4-Butyl	O	7.0
11	11	CH_3	CH_3	2-Butyl	O	1.5
12	12	CH_3	CH_3	4-F	O	4.9
13	13	CH_3	CH_3	2-F	O	2.4
14	14	CH_3	CH_3	3-F	O	4.5
15	15	CH_3	CH_3	4-CH_2CH_2OH	O	2.9
16	16	CH_3	CH_3	4-OCH_3	O	2.2
17	17	CH_3	CH_3	2-OCH_3	O	6.2
18	18	CH_3	CH_3	3-OCH_3	O	3.6
19	19	CH_3	CH_3	4-OPh	O	22.7
20	20	CH_3	CH_3	2-OPh	O	15.8
21	21	CH_3	CH_3	3-OPh	O	3.9
22	22	CH_3	CH_3	4-$NHCOCH_3$	O	6.1
23	23	CH_3	CH_3	3-$NHCOCH_3$	O	2.3
24	24	CH_3	CH_3	2-NO_2	O	17.5
25	25	CH_3	CH_3	4-CH_2CH_3	O	2.8
26	26	CH_3	CH_3	2-CH_2CH_3	O	1.6
27	27	CH_3	CH_3	3-CH_2CH_3	O	8.2
28	28	CH_3	CH_3	4-CH_2OH	O	1.7
29	29	CH_3	CH_3	2-CH_2OH	O	11.1
30	30	CH_3	CH_3	3-CH_2OH	O	2.4
31	31	CH_3	CH_3	2-CF_3	O	3.9
32	32	CH_3	CH_3	3-CF_3	O	2.8
33	33	CH_3	CH_3	4-OCH_2CH_3	O	3.2
34	34	CH_3	CH_3	2-OCH_2CH_3	O	3.4
35	35	CH_3	CH_3	H	O	5.7
36	36	H	H	H	O	0.35
37	37	CH_3	CH_3	3-$COOCH_3$	O	2.1
38	38[a]	CH_3	CH_3	4-CF_3	O	>100

[a] Molecule 38 was not included in the CoMFA analysis, used only for LeapFrog calculations.

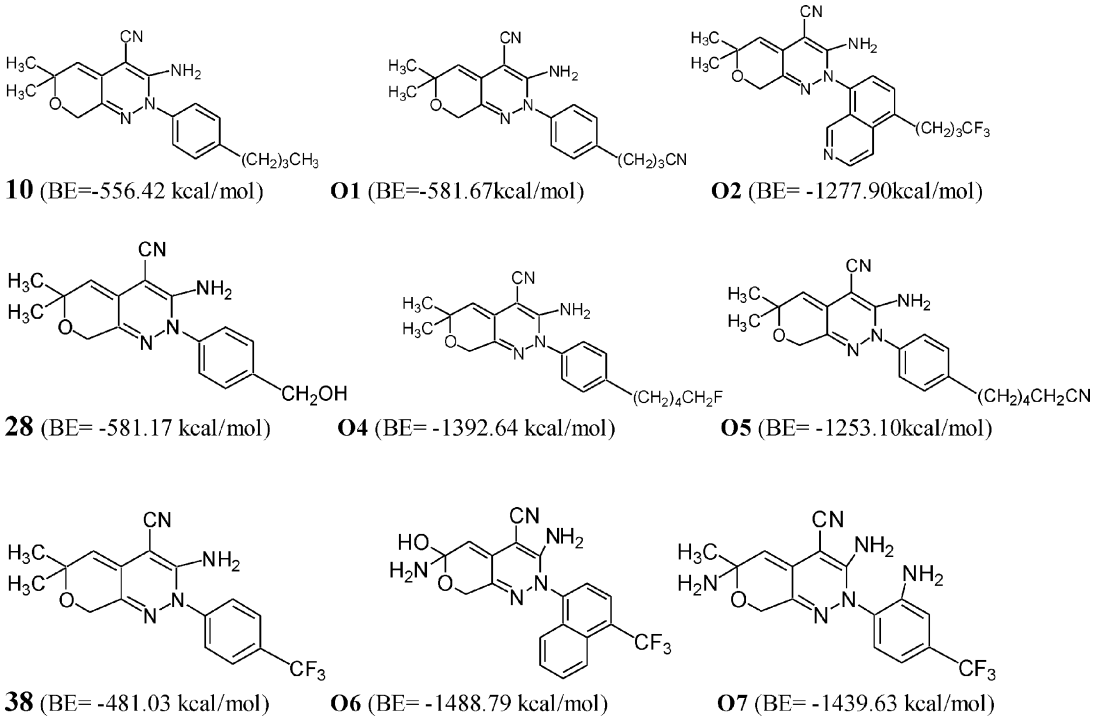

Scheme 1. Set of optimized molecules by LeapFrog.

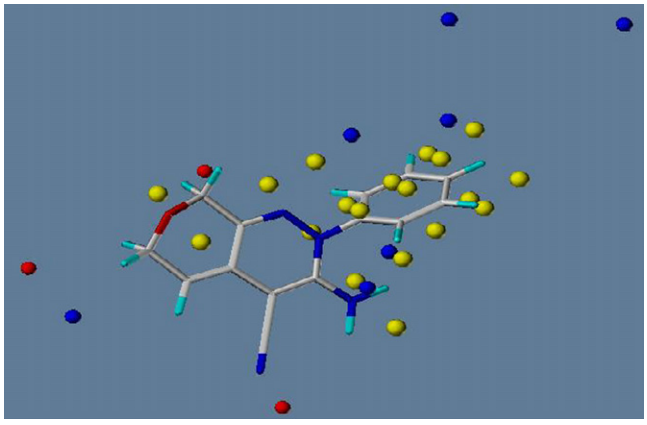

Fig. 5. The site points generated by LeapFrog along with molecule 36.

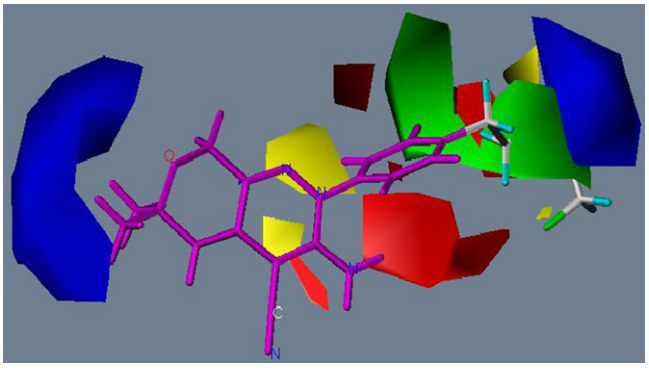

Fig. 6. One of the optimized molecules O4 is shown in the CoMFA contours. Magenta shows the backbone of the reference molecule while Sybyl type atom colors show the optimized part of the molecule.

optimized part of the molecule. The figure shows how the bulky substituent goes further into the steric field (green) of the CoMFA contours and exhibits higher binding energy. Using this concept of hypothetical cavity generation, many molecules were optimized and subjected to further analysis.

4. Conclusions

The 3D-QSAR analysis, CoMFA was used to build statistically significant model with good correlative power for PTP1B inhibitory activities of the pyridazine derivatives. The robustness of the derived models was verified by bootstrapping method. The CoMFA model has been developed particularly on non-competitive inhibitors of PTP1B. The result of this study may provide a base for developing selective inhibitors of PTP1B. LeapFrog was an attempt to design molecules based on the concept of hypothetical cavity generation using CoMFA contours. A few molecules optimized by this approach are included in the study. More potent and selective inhibitors, which would act non-competitively on PTP1B can be designed using this model, however, such works need to be supported by synthesis.

Acknowledgement

MES thanks Department of Science and Technology (DST), New Delhi for the Fast Track Young Scientist Project grant.

References

[1] C.J. Bailey, Insulin resistance and anti diabetic drugs—treating a moving target, Biochem. Pharmacol. 58 (1999) 1511–1520.

[2] J. Montalibet, B.P. Kennedy, Therapeutic strategies for targeting PTP1B in diabetes, Drug Discov. Today: Therap. Strat. 2 (2005) 129–135.
[3] B.P. Kennedy, Role of protein tyrosine phosphatase-1B in diabetes and obesity, Biomed. Pharmacother. 53 (1999) 466–470.
[4] J.C. Byon, A.B. Kusari, J. Kusari, Protein-tyrosine phosphatase-1B acts as a negative regulator of insulin signal transduction, Mol. Cell. Biochem. 2 (1998) 101–108.
[5] M. Elchebly, P. Payette, E. Michaliszyn, W. Cromlish, S. Collins, A.L. Loy, D. Normandin, A. Cheng, J. Himms-Hagen, C.C. Chan, C. Ramachandran, M.J. Gresser, M.L. Tremblay, B.P. Kennedy, Increased insulin sensitivity and obesity resistance in mice lacking the protein tyrosine phosphatase-1B gene, Science 283 (1999) 1544–1548.
[6] L.D. Klaman, O. Boss, O.D. Peroni, J.K. Kim, J.L. Martino, J.M. Zabolotny, N. Moghal, M. Lubkin, Y.B. Kim, A.H. Sharpe, A. Stricker-Krongrad, G.I. Shulman, B.G. Neel, B.B. Kahn, Increased energy expenditure, decreased adiposity, and tissue-specific insulin sensitivity in protein-tyrosine phosphatase 1B-deficient mice, Mol. Cell. Biol. 20 (2000) 5479–5489.
[7] G. Liu, Protein tyrosine phosphatase 1B inhibition: opportunities and challenges, Curr. Med. Chem. 10 (2003) 1407–1421.
[8] M.S. Malamas, J. Sredy, C. Moxham, A. Katz, W. Xu, R. McDevitt, F.O. Adebayo, D.R. Sawicki, D.S. Seestaller, J.R. Taylor, Novel benzofuran and benzothiophene biphenyls as inhibitors of protein tyrosine phosphatase 1B with anti hyperglycemic properties, J. Med. Chem. 43 (2000) 1293–1310.
[9] J.H. Ahn, S.Y. Cho, J.D. Ha, S.Y. Chu, S.H. Jung, Y.S. Jung, J.Y. Baek, I.K. Choi, E.Y. Shin, S.K. Kang, Synthesis PTP1B inhibition of 1,2-naphthoquinone derivatives as potent anti-diabetic agents, Bioorg. Med. Chem. Lett. 12 (2002) 1941–1946.
[10] M.S. Malamas, J. Sredy, I. Gunawan, B. Mihan, D.R. Sawicki, L. Seestaller, D. Sullivan, B.R. Flam, New azolidinediones as inhibitors of protein tyrosine phosphatase 1B with antihyperglycemic properties, J. Med. Chem. 5 (2000) 995–1010.
[11] J. Wrobel, J. Sredy, C. Moxham, A. Dietrich, Z. Li, D.R. Sawicki, L. Seestaller, L. Wu, A. Katz, D. Sullivan, C. Tio, Z.Y. Zhang, PTP1B inhibition and antihyperglycemic activity in the ob/ob mouse model of novel 11-arylbenzo[b]naphtho[2,3-d]furans and 11-arylbenzo[b]-naphtho[2,3-d]thiophenes, J. Med. Chem. 42 (1999) 3199–3202.
[12] S. Desmarais, R.W. Friesen, R. Zamboni, C. Ramachandran, [Difluro(phosphono)methyl]phenylalanine-containing peptide inhibitors of protein tyrosine phosphatases, Biochem. J. 337 (1999) 219–223.
[13] Z. Xin, T. Oost, C. Abad-Zapatero, P. Hajduk, Z. Pei, B.G. Szczepankiewicz, C.W. Hutchins, S.J. Ballaron, M.A. Stashko, T. Lubben, Potent, selective inhibitors of protein tyrosine phosphatase 1B, Bioorg. Med. Chem. Lett. 13 (2003) 1887–1890.
[14] T.R. Burke Jr., Z.Y. Zhang, Protein-tyrosine phosphatases: structure, mechanism, and inhibitor discovery, Biopolymers 47 (1998) 225–241.
[15] S.D. Larsen, T. Barf, C. Liljebris, P.D. May, D. Ogg, T.J. O'Sullivan, B.J. Palazuk, H.J. Schostarez, F.C. Stevens, J.E. Bleasdale, Synthesis and biological activity of a novel class of small molecular weight peptidomimetic competitive inhibitors of protein tyrosine phosphatase 1B, J. Med. Chem. 45 (2002) 598–622.
[16] M.O. Taha, M.A. AlDamen, Effects of variable docking conditions and scoring functions on corresponding protein-aligned comparative molecular field analysis models constructed from diverse human protein tyrosine phosphatase 1B inhibitors, J. Med. Chem. 48 (2005) 8016–8034.
[17] M. Zhou, M. Ji, Molecular docking and 3D-QSAR on 2-(oxalylamino) benzoic acid and its analogues as protein tyrosine phosphatase 1B inhibitors, Bioorg. Med. Chem. Lett. 15 (2005) 5521–5525.
[18] V.S. Murthi, V.M. Kulkarni, 3D-QSAR CoMFA and CoMSIA on protein tyrosine phosphatase 1B inhibitors Bioorg, Med. Chem. 10 (2002) 2267–2282.
[19] M.E. Sobhia, P.V. Bharatam, Comparative molecular similarity indices analysis (CoMSIA) studies of 1,2-naphthoquinone derivatives as PTP1B inhibitors, Bioorg. Med. Chem. 13 (2005) 2331–2338.
[20] A. Martinez, M. Alonso, A. Castro, I. Dorronsoro, J.L. Gelpi, F.J. Luque, C. Perez, F.J. Moreno, SAR and 3D-QSAR studies on thiadiazolidinone derivatives: exploration of structural requirements for glycogen synthase kinase 3 inhibitors, J. Med. Chem. 48 (2005) 7103–7112.
[21] SYBYL Ligand-Based Design Manual version 7.1, Tripos Inc., St. Louis, MO.
[22] M. Makhija, R.T. Kasliwal, V.M. Kulkarni, N. Neamati, De novo design and synthesis of HIV-1 integrase inhibitors, Bioorg. Med. Chem. 12 (2004) 2317–2333.
[23] D.B. Jordan, G.S. Basarab, D. Liao, W.M. Johnson, K.N. Winzenberg, D.A. Winkler, Structure based design of inhibitors of the rice blast fungal enzyme trihydroxynaphthalene reductase, J. Mol. Graphics Modell. 19 (2001) 434–447.
[24] C. Liljebris, J. Martinsson, L. Tedenborg, M. Williams, E. Barker, J.E. Duffy, A. Nygren, S. James, Synthesis and biological activity of a novel class of pyridazine analogues as non-competitive reversible inhibitors of protein tyrosine phosphatase 1B (PTP1B), Bioorg. Med. Chem. 10 (2002) 3197–3212.
[25] SYBYL Molecular Modeling System, version 7.1, Tripos Inc., St. Louis, MO, 63144-2913.
[26] J. Gasteiger, M. Marsili, Iterative partial equalization of orbital electro negativity—a rapid access to atomic charges, Tetrahedron 36 (1980) 3219–3228.
[27] M.J.D. Powell, Restart procedures for the conjugate gradient method, Math. Program. 12 (1977) 241–254.
[28] R.D. Cramer, D.E. Patterson, J.D.J. Bunce, Comparative molecular field analysis (CoMFA) 1. Effect of shape on binding of steroids to carrier proteins, J. Am. Chem. Soc. 110 (1988) 5959–5967.
[29] R.D. Cramer, J.D. Bunce, D.E. Patterson, Crossvalidation, bootstrapping, and partial least squares compared with multiple regression in conventional QSAR studies quant, Struct. -Act. Relat. 7 (1988) 18–25.
[30] M. Clark, R.D. Cramer III, D.M. Jones, D.E. Patterson, P.E. Simeroth, Comparative molecular field analysis (CoMFA) 2. Toward its use with 3D-structural databases, Tetrahedron Comput. Methodol. 3 (1990) 47–59.
[31] P.J. Goodford, A computational procedure for determinging energetically favourable binding sites on biologically important macromolecules, J. Med. Chem. 28 (1985) 849–857.